Pulsed three-dimensional electron spin resonance microscopy

Aharon Blank, Curt R. Dunnam, Peter P. Borbat, and Jack H. Freed[a)]
National Biomedical Center for Advanced ESR Technology, Department of Chemistry and Chemical Biology, Cornell University, Ithaca, New York 14853

(Received 6 August 2004; accepted 14 October 2004)

A three-dimensional (3D) electron spin resonance (ESR) microimaging system, operating in pulse mode at 9 GHz is presented. This microscope enables the acquisition of spatially resolved magnetic resonance signals of free-radicals in solid or liquid samples with a resolution of up to $\sim 3.5\times 7\times 11.4$ μm in 20 min of acquisition. The detection sensitivity at room temperature is $\sim 1.2\times 10^9$ spins/$\sqrt{\text{Hz}}$, which enables the measurement of $\sim 2\times 10^7$ spins in each voxel after 60 min of acquisition. The resolution and detection sensitivity are the best obtained so far for ESR at ambient conditions of temperature and pressure. This ESR microscope can be employed in the investigation of a variety of samples in the fields of botany, life sciences, and materials science. © *2004 American Institute of Physics*. [DOI: 10.1063/1.1828599]

High resolution electron spin resonance (ESR) imaging of microscopic samples is an emerging field, which adapts traditional nuclear magnetic resonance (NMR) imaging techniques to modern ESR technology.[1–4] The goal of this method is to obtain routine magnetic resonance images of biological specimens or samples for materials science applications, with a spatial resolution of less than 1 μm in a few minutes of acquisition. Conventional magnetic resonance microscopy is currently dominated by NMR, which is a well developed technique but is limited, due to signal-to-noise-ratio (SNR) and molecular diffusion, to a practical resolution of $\sim(10\ \mu\text{m})^3$.[1,5–7] With its potential advantages over NMR, ESR could become the technique of choice for microscopic magnetic resonance imaging applications.[4] An ESR microscope can provide similar information to that obtained from NMR measurements,[3,4] (i.e., spin concentration, T_1, T_2, and diffusion contrast), which has many capabilities and provides complimentary information to conventional optical and fluorescence confocal microscopy.[3,8] Since most samples do not contain stable free radicals, these paramagnetic species are added in a manner similar to that of the contrast agents employed in NMR or dyes in optical microscopy.

Recently, we have developed a 3D ESR microscope operating in continuous wave (CW) mode, at 9 GHz.[4] This system is capable of obtaining 3D images of $64\times 64\times 64$ voxels with a resolution of $\sim 10\times 10\times 30$ μm at $\sim$60 min of acquisition. ESR imaging in the cw mode is a powerful technique compatible with a variety of samples and radicals with relatively broad lines.[9] However, it suffers from some drawbacks, which may limit its potential use in some cases. For example, the cw mode requires longer image acquisition times (or has reduced SNR for the same acquisition time);[9] It cannot directly obtain image contrasts such as T_1, T_2, and diffusion (only T_2^* can be derived from the linewidth); and the time resolution of the cw mode is low, which prevents the imaging of short lived radicals (for example, light induced radicals). To overcome these limitations, we have developed a pulsed 9 GHz ESR microscopy system, reported here.

The pulsed ESR microscope is described schematically in Fig. 1, and a typical imaging sequence is shown in Fig. 2. In contrast to NMR, the short time scale of the ESR experiment (ns–μs) makes it difficult to employ many pulsed imaging techniques, since we require short microwave pulses, short, and intense pulsed field gradients, and a fast acquisition and data averaging system. The system is built from the following main components: (a) Standard PC which controls the overall image acquisition process through the user interface of LabView software (National Instruments); (b) timing system (Model 100-24, SpinCore), which has 24 TTL outputs, time resolution of 10 ns, programming time of ~ 10 μs and a minimum pulse length of 50 ns; (c) an 8 bit PCI-format digitizer card for raw data acquisition and averaging (AP-240, Acqiris), which has two channels, and a sampling rate of 1 GHz; it can average up to 0.7 M waveforms/s (d) PCI analog output card with four outputs (PCI-6711, National Instruments); (e) microwave reference source (HP8620C) with power output of 10 dBm in the 2–18 GHz range; (f) a "home-built" pulsed microwave bridge containing a 6–17 GHz low power transceiver (g), and a solid-state power amplifier (h) with 0.25 W output, 35 dB gain (Genesis). The homodyne transceiver incorporates one transmission channel with biphase modulation, which controls the individual pulse phase (e.g., 0° or 180° for echo phase cycling). The timing system triggers the transmission pulses, determines the bimodulator phase, and provides triggers for the diode protection of the receiver while transmitting the high power pulses. The relatively low power output of the transceiver is sufficient to provide hard 90° pulses of $\sim$80 ns with the small resonator we employ (see below).[4] The pulsed gradient coils in the imaging probe are driven by a pair of gradient coil drivers (j) fed by preregulated high voltage

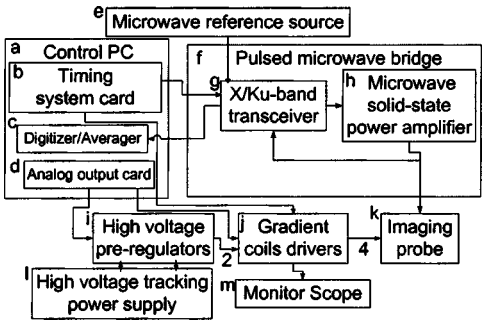

FIG. 1. Block diagram of the pulsed imaging system.

[a)]Electronic mail: jhf3@cornell.edu

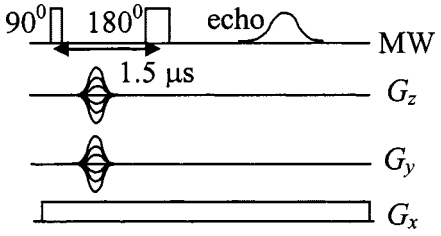

FIG. 2. Typical imaging sequences employed in the pulsed ESR microimaging system, based on a simple primary echo with constant gradient that encodes the spins along the *x* axis, and two phase gradients for encoding the information on the *yz* plane (Ref. 2). This sequence can be repeated every $\sim T_1$. Due to limits in amplifier power, we employed two 90° pulses (80 ns) rather than 90° and 180° pulses.

power supplies. The gradient coils driver has four channels. Two of the channels can generate large (up to ~8 A peak) half-sine current pulses by precharging a capacitor and subsequently discharging it into the gradient coil.[10] The two remaining channels produce constant dc current into the "*x*-axis" gradient coils and into a bias coil, producing a dc field which is used to lock the magnetic field on the resonance frequency of the spins. The lock error term is generated by occasionally sampling the FID signal without any gradients and correcting for observed field drift.[4] The imaging probe (*k*), shown in Fig. 3, is similar in key aspects to the 9 GHz 3D probe employed for cw ESR imaging, which is described in detail in Ref. 4. The main differences between the cw and the pulsed probes are in the structure of the gradient coils and the microwave resonator shield. The *y*- and *z*-axis gradient coils (based on Golay geometry[11]) are optimized for pulsed currents, and have relatively small inductance of 6.5 μH. They produce gradients of 1.6 and 1.1 T/m A (for the *y* and *z* axis respectively, measured with a pickup coil at 1 MHz), when the coil pairs are connected in parallel. The *x*-axis gradient coil (Maxwell pair) operates in dc mode, and has a self-inductance of 90 μH, and a gradient efficiency of 3.5 T/m A. A very thin gold foil (~0.2 μm) is used as a shield between the structure of the coils and the microwave resonator. This prevents the microwave field from escaping the resonator structure, while simultaneously enabling the transmission of the magnetic field pulse gradients into the resonator structure and also minimizing potentially disturbing eddy currents. The resonator has a loaded

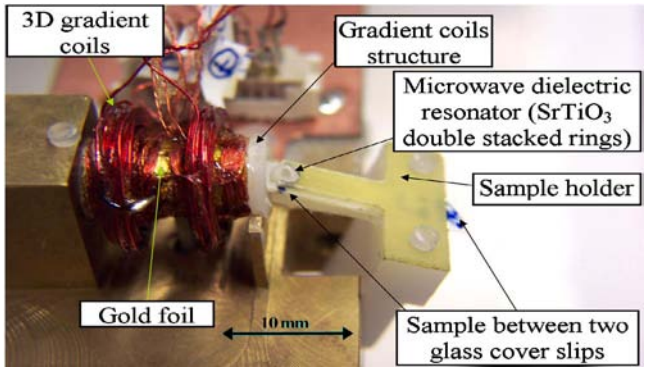

FIG. 3. (Color online) Image of the pulsed imaging probe, with the resonator structure taken outside the gradient coils. The probe structure and microstrip coupling scheme (not shown) follows closely the cw probe, which is described in detail in Ref. 4, but with modified gradient coils and a thin gold foil to shield the microwave structure.

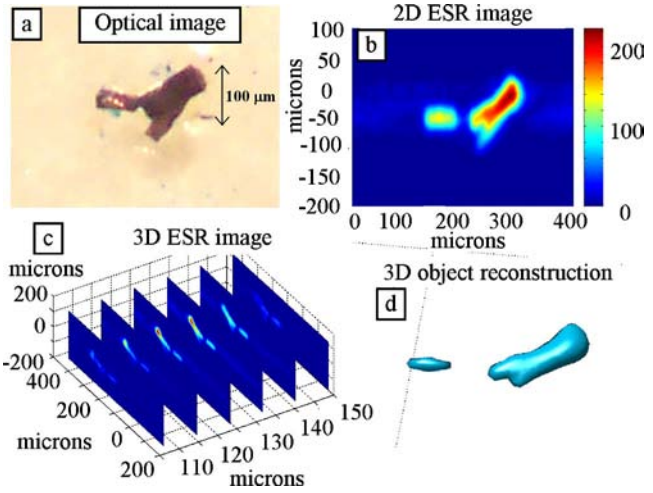

FIG. 4. (Color online) Optical and ESR images of LiPc crystal: (a) the optical image of the crystal; (b) 2D ESR image (acquired without any *z*-axis gradients); (c) 3D ESR image, showing several slices along the *z* axis; (d) reconstruction of the object with the 3D ESR signal information.

quality factor at a critical coupling of ~400, and an effective volume of ~3 mm^3.[3,4]

The performance of the system was verified with respect to theoretical predictions of SNR and image resolution.[3] First, the SNR was measured for a 0.05 mm^3 sample of 1 mM water solution of protonated trityl radical[12] containing $\sim 3\times10^{13}$ spins. The measured single shot FID SNR (without any gradients) of ~100 agrees well with the theoretical prediction [Ref. 3, Eq. (13)], of ~75 for this small sample. This corresponds to detection sensitivity at room temperature of $\sim 1.2\times10^9$ spins/$\sqrt{\text{Hz}}$, which enables the measurement of $\sim 2\times10^7$ spins in each voxel after 60 min of acquisition. Next, the image SNR and resolution were estimated with two types of test samples: (1) Lithium phthalocyanine (LiPc) phantom: A small crystal of LiPc (the same sample that was used in our previous cw work[3,4]) was used as a high-spin-concentration solid test sample. The corresponding optical and ESR images appear in Fig. 4. The 3D image of $256\times256\times50$ voxels was acquired in 20 min. The constant *x* gradient employed (3 T/m) corresponds to a resolution of ~3.5 μm [Eq. (14) in Ref. 3, with $T_2^*$of 1.1 μs]. The *y*-gradient produced half sine waves (Fig. 2) with an amplitude of 4.5 A(=7.2 T/m), and half period of 1.1 μs corresponds to a resolution of ~7 μm [Ref. 3, Eq. (15)], and the *z* gradient (employed with maximum 4 A=4.4 T/m), corresponds to a resolution of ~11.4 μm. The single voxel SNR is ~700. This crystal contains $\sim10^8$ spins per (1 μm)^3, or $\sim 2.8\times10^{10}$ spins per imaged voxel, which agrees well with the SNR predictions and measurements described above. The resolution for such a sample is limited by the strength of the gradients we currently employ and not by the SNR. (2) Trityl solution in a nylon mesh: A 1 mM trityl solution was placed in a woven nylon mesh (Goodfellow) with mesh aperture of 50×50 μm and wire diameter of 39 μm.[3] This type of sample has well-defined 3D geometry and known spin concentration. The corresponding optical and ESR images appear in Fig. 5. The 3D image of $256\times256\times50$ voxels was acquired after 40 min. The theoretical image resolution (based on the amplitude of the field gradients, which was smaller than in the previous example) is $8.8\times10.5\times19$ μm. The actual resolution may be estimated from the

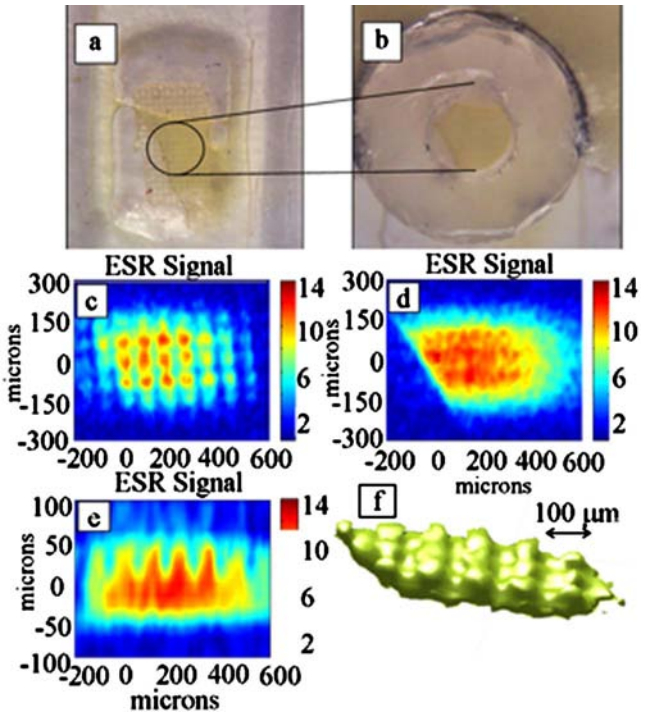

FIG. 5. (Color online) Optical and ESR images of trityl solution in a nylon mesh: (a),(b) the optical images showing the circular area inside the imaging probe [grey ring in (b), i.d.=0.81 mm]; (c) a single *z* slice of the 3D ESR image showing the mesh plane; (d) another *z* slice which corresponds to the plane of the solution below the mesh; (e) a vertical cut through the sample (*zy* plane); (f) a reconstruction of the total solution volume. The sample *y* axis is the horizontal axis in the images (c)–(e). The limited bandwidth of excitation (two 80 ns pulses), restricts the image extent along the *x* axis, while the *y* extent is limited by the resonator size.

unique features of the sample as they resolve in the ESR image. If we adopt the Rayleigh resolution criterion,[1] we should be able to resolve in the *xy*-plane two ~ 10 μm voxels with signal separated by an ~ 10 μm voxel without signal.[13] The current sample is not fine enough to directly obtain such information but it readily shows excellent separation between the 50 μm voxels separated by the 39 μm wires. The separation along the *y* axis is of better quality than that along the *x* axis. This is due to the Lorentzian line shape that decreases very slowly and results in a less resolved image for constant gradients than in the case of phase gradients.[14] The *z*-axis shows good separation along the sample (~ 90 μm high), where in the lower part of the image, only the solution is observed, and on the upper part, the ~ 39 μm high mesh is visible. Thus, in terms of resolution, we can conclude (for both samples) that the theoretical image resolution (as obtained from the measured field gradients), may very well be the actual measured image resolution, but direct evidence can only be obtained with specially prepared 3D test samples. In terms of SNR, the single voxel SNR of ~ 40 is in good agreement with the predicted/measured results; [there are $\sim 6 \times 10^5$ spins per $(1\ \mu\text{m})^3$, or $\sim 10^9$ spins per imaged voxel].

The high spatial resolution and SNR, large image size, and short acquisition time of our system are the current state-of-the-art of any ESR microscopy technique, which is readily applicable to a range of biological, botanical, and materials science applications. The theoretical predictions,[3] confirmed by our microscope, indicate that even greater resolution, approaching 1 μm, may be achievable by working at higher ESR frequencies. Other experiments have previously demonstrated better resolution than we obtained in the present work, through conventional NMR techniques,[6] or by magnetic resonance force microscopy (MRFM).[15,16] In addition, Hall detection,[17] microcoils,[18] and surface probes,[19] may be useful in the future for high resolution magnetic resonance imaging. However, all these methods can be employed only to a very limited extent when biologically related, or relatively thick samples are considered. Thus, for example, in conventional NMR the actual "practical" resolution for several minutes of acquisition is $>(10\ \mu\text{m})^3$ with very limited image size.[7,20] MRFM suffers from low 3D sensitivity, especially when the samples are thicker than a few microns. Furthermore, it requires extreme physical conditions (high vacuum and often low temperatures), and complicated sample preparation. These collective constraints make MRFM (as well as other surface scanning methods[21]), at its present stage, unpractical for most biological and thick sample applications. Other detection methods, as mentioned above,[17–19] have yet to provide high resolution 3D images.

This research was supported by grants from NIH/NCRR and NSF Chemistry.

[1] P. T. Callaghan, *Principles of Nuclear Magnetic Resonance Microscopy* (Oxford University Press, Oxford, 1991).
[2] A. Feintuch, G. Alexandrowicz, T. Tashma, Y. Boasson, A. Grayevsky, and N. Kaplan, J. Magn. Reson. **142**, 382 (2000).
[3] A. Blank, C. R. Dunnam, P. P. Borbat, and J. H. Freed, J. Magn. Reson. **165**, 116 (2003).
[4] A. Blank, C. R. Dunnam, P. P. Borbat, and J. H. Freed, Rev. Sci. Instrum. **75**, 3050 (2004).
[5] S. Gravina and D. G. Cory, J. Magn. Reson., Ser. B **104**, 53 (1994).
[6] L. Ciobanu, D. A. Seeber, and C. H. Pennington, J. Magn. Reson. **158**, 178 (2002).
[7] L. Ciobanu and C. H. Pennington, Solid State Nucl. Magn. Reson. **25**, 138 (2004).
[8] D. D. Stark and W. G. Bradley, *Magnetic Resonance Imaging*, 2nd ed. (Mosby, St. Louis, MO, 1992).
[9] *EPR Imaging and In Vivo EPR*, edited by G. R. Eaton, S. S. Eaton, and K. Ohno (CRC, Boca Raton, 1991).
[10] M. S. Conradi, A. N. Garroway, D. G. Cory, and J. B. Miller, J. Magn. Reson. (1969-1992) **94**, 370 (1991).
[11] J.-M. Jin, *Electromagnetic Analysis and Design in Magnetic Resonance Imaging* (CRC, Boca Raton, 1999).
[12] J. H. Ardenkjaer-Larsen, I. Laursen, I. Leunbach, G. Ehnholm, L. G. Wistrand, J. S. Petterson, and K. Golman, J. Magn. Reson. **133**, 1 (1998).
[13] In previous high resolution magnetic resonance microscopy papers, the resolution was estimated by the rate of signal decrease from areas with signal to areas without signal (Refs. 3, 4, and 6). This approach is very crude and does not hold for high SNR, since the signal in the empty voxels will not be dominated by noise but rather by the margins of the point spread function of the voxel with the signal in it. Here we try to adopt a more accurate definition but which requires well defined 3D test samples.
[14] G. G. Maresch, M. Mehring, and S. Emid, Physica B & C **138**, 261 (1986).
[15] S. Tsuji, T. Masumizu, and Y. Yoshinari, J. Magn. Reson. **167**, 211 (2004).
[16] S. H. Chao, W. M. Dougherty, J. L. Garbini, and J. A. Sidles, Rev. Sci. Instrum. **75**, 1175 (2004).
[17] G. Boero, P. A. Besse, and R. Popovic, Appl. Phys. Lett. **79**, 1498 (2001).
[18] G. Boero, M. Bouterfas, C. Massin, F. Vincent, P. A. Besse, R. S. Popovic, and R. S. Schweiger, Rev. Sci. Instrum. **74**, 4794 (2003).
[19] F. Sakran, A. Copty, M. Golosovsky, N. Bontemps, D. Davidov, and A. Frenkel, Appl. Phys. Lett. **82**, 1479 (2003).
[20] L. Ciobanu, A. G. Webb, and C. H. Pennington, Prog. Nucl. Magn. Reson. Spectrosc. **42**, 69 (2003).
[21] C. Durkan and M. E. Welland, Appl. Phys. Lett. **80**, 458 (2002).